Two New Antimony(III) Chloride Hybrids Composed of Mononuclear $[SbCl_6]^{3-}$ Unit and Ionic Liquid Cations with Different Length of Alkyl Chain①

ZHANG Zhi-Zhuan[a, b] JIN Jian-Ce[b] GONG Liao-Kuo[b②]
DU Ke-Zhao[a] HUANG Xiao-Ying[b②]

[a] (*College of Chemistry and Materials Science, Fujian Normal University, Fuzhou* 350007, *China*)

[b] (*State Key Laboratory of Structural Chemistry, Fujian Institute of Research on the Structure of Matter, Chinese Academy of Sciences, Fuzhou* 350002, *China*)

ABSTRACT Two new hybrid chloroantimonates, namely, $[Prmim]_3SbCl_6$ (**1**, Prmim = 1-propyl-3-methylimidazolium) and $[Hmim]_3SbCl_6$ (**2**, Hmim = 1-hexyl-3-methylimidazolium), were synthesized in ionic liquids (ILs) with the yields of 97% and 72%, respectively. Single-crystal X-ray diffraction (SCXRD) study reveals that **1** crystallizes in monoclinic, space group *Pn* with a = 15.2988(12), b = 13.6388(10), c = 15.6761(13) Å, β = 98.677(7)°, V = 3233.5(4) Å^3, Z = 4, D_c = 1.459 g cm^{-3}, F(000) = 1440, μ = 1.370 mm^{-1}, R = 0.0589 and wR = 0.1366 ($I > 2\sigma(I)$); **2** crystallizes in the hexagonal space group of $P6_3$ with a = 27.7471(6), b = 27.7471(6), c = 8.9811(2) Å, V = 5988.2(3) Å^3, Z = 6, D_c = 1.391 g cm^{-3}, F(000) = 2592, μ = 1.121 mm^{-1}, R = 0.0420 and wR = 0.0726 ($I > 2\sigma(I)$). The photophysical properties of the title compounds were studied by solid-state optical absorption, photoluminescent excitation/emission (PLE/PL), PL decay spectra and photoluminescent quantum yield (PLQY). **1** and **2** exhibit PL peaks at 627 and 607 nm, Stokes shifts of 257 and 242 nm, and PLQY of 32.5% and 49.2%, respectively. The distinct photo physical characteristics of **1** and **2** are highly related to the distortion extent of the $[SbCl_6]^{3-}$ unit.

Keywords: antimony(III) chloride, ionic liquid, luminescence, distortion;
DOI: 10.14102/j.cnki.0254–5861.2011–3099

1 INTRODUCTION

Inorganic-organic hybrid metal halides (IOMHs) have received increasing attention because of their superior photophysical characteristics with potential applications in photovoltaics, solid-state lighting, *etc.*[1-10]. Zero dimensional (0*D*) IOMHs with structurally and electronically isolated halometallate species generally exhibit broadband emission mainly due to self-trapped excitons (STE) from the interaction of excitons with lattice and large structural reorganization in the excited state[11-14]. The STE emission has been observed in the hybrid compounds based on the metal ion with ns^2 electron configuration, such as, Ge^{2+}, Sn^{2+}, Pb^{2+}, Sb^{3+} and Bi^{3+}[15-31].

Sb^{3+} coordinating with halogen ions X^- (X = Cl, Br, I) can form haloantimonate(III) anions with rich structural moieties like $[SbX_4]^-$[32], $[SbX_5]^{2-}$[31, 33-41], $[SbX_6]^{3-}$[38, 42], $[Sb_2X_7]^-$[43], $[Sb_2X_8]^{2-}$[44], $[Sb_2X_9]^{3-}$[45, 46], $[Sb_2X_{10}]^{4-}$[47] and $[Sb_2X_{11}]^{5-}$[48]. Among them, the mononuclear $[SbCl_5]^{2-}$ unit is commonly used to construct photoluminescent (PL) 0*D*-IOMHs. Such IOMHs generally exhibit broadband emission over a wide range of spectrum originating from $^3P_1 \rightarrow {}^1S_0$ transition[31, 33-41], mostly with a near-unity PL quantum yield (PLQY), *e.g.*, in $(C_9NH_{20})_2SbCl_5$ (C_9NH_{20} = 1-butyl-1-methylpyrrolidinium)[40], $(TEBA)_2SbCl_5$ (TEBA = benzyltriethylammonium)[31], $(Ph_4P)_2SbCl_5$ (Ph_4P = tetraphenylphosphonium)[41], and $(PPN)_2SbCl_5$ (PPN = bis(triphenylphosphoranylidene) ammonium cation)[33]. The high PL efficiency might be attributed to the sufficient separation of the neighboring $[SbCl_5]^{2-}$ units by cations leading to little-to-no interactions

Received 17 January 2021; accepted 28 January 2021 (**CCDC 2055082 for 1 and 2055083 for 2**)

① This work was supported by the National Natural Science Foundation of China (No. 21671187) and the Natural Science Foundation of Fujian Province (No. 2020J01118)

② Corresponding authors. E-mails: xyhuang@fjirsm.ac.cn and lkgong@fjirsm.ac.cn

or electronic band formation[40]. Additionally, dual emission as well as white light emission in compounds $(Bmim)_2SbCl_5$ (Bmim = 1-butyl-3-methlimidazolium) and $(TTA)_2SbCl_5$ (TTA = tetraethylammonium) could be easily and conveniently realized by adjusting the excitation wavelength[31, 39]. By introducing H_2O molecules to expand the distance between $[SbCl_5]^{2-}$ species and create more local photoelectrons for the $[SbCl_5]^{2-}$ species, the PLQY of 25.3% in $(C_6N_2H_{16})_2SbCl_5$ ($C_6N_2H_{16}$ = 2,6-dimethylpiperazine) could be enhanced to 39.6% in $(C_6N_2H_{16})_2SbCl_5 \cdot H_2O$[36]. These compounds have shown potential applications in emerging fields such as thermal imaging analysis[34], scintillator[33] and anti-counterfeiting luminescent paper[37, 38]. 0*D*-IOMHs with mononuclear $[SbCl_6]^{3-}$ unit also have been widely reported based on CCDC database. However, their PL properties have been rarely demonstrated[38, 42]. Recently, it has been reported that $(Bzmim)_3SbCl_6$ (Bzmim = 1-benzyl-3-methylimidazolium) could exhibit green emission with high PLQY of 87.5%[38].

Ionic liquids (ILs), as a kind of "green" reagents and templates, exhibit various excellent properties, such as low volatility, large liquid ranges, nonflammability, and high stability[49-52]. Additionally, a wide variety of ILs and various substitution ways on the parent rings provide favorable conditions for obtaining diverse structures[53-55]. Herein, by using imidazolium based ILs with different-length alkyl chain as the solvent and template, two new hybrid chloroantimonates, namely, $[Prmim]_3SbCl_6$ (**1**, Prmim = 1-propyl-3-methylimidazolium) and $[Hmim]_3SbCl_6$ (**2**, Hmim = 1-hexyl-3-methylimidazolium), were synthesized. Both feature a 0*D* structure with isolated $[SbCl_6]^{3-}$ octahedron as confirmed by single-crystal X-ray diffraction (SCXRD). Under the excitation wavelength of 370 nm, **1** exhibits orange emission peak at 627 nm with a large Stokes shift of 257 nm, while **2** exhibits orange-yellow emission peak at 607 nm with a large Stokes shift of 242 nm excited at 365 nm. The PLQY for **1** and **2** are 32.5% and 49.2%, respectively. The distinct photophysical properties (emission peak, Stokes shift, and PLQY) of two compounds are revealed to be related to the distortion of isolated $[SbCl_6]^{3-}$ octahedron by comparing the title $[SbCl_6]^{3-}$ unit with those reported in literature[38, 42].

2 EXPERIMENTAL

Antimony(III) chloride ($SbCl_3$, 99%) was purchased from Adamas Reagent Co., Ltd. [Prmim]Cl (99%) and [Hmim]Cl (99%) were purchased from Lanzhou GreenChem ILs, LICP, CAS (Lanzhou, China). All the reagents were utilized without further purification.

Powder X-ray diffraction (PXRD) patterns were recorded on a Rigaku Miniflex II diffractometer with Cu*Kα* radiation (λ = 1.54178 Å) at room temperature. Elemental analyses (EA) for C, H and N were conducted on a German Elementary Vario MICRO instrument. Thermogravimetric (TG) analysis was performed on a NETZSCH STA 449F3 instrument at a heating rate of 10 K·min^{-1} under a N_2 atmosphere from 20 to 800 ℃. Solid-state optical diffuse reflectance spectra were performed at room temperature on a Shimadzu 2600 UV/Vis spectrometer in a range of 200～800 nm. $BaSO_4$ with 100% reflectance was used as a standard. The absorption data were obtained from reflectance spectra by using the Kubelka-Munk function $\alpha/S = (1 - R)^2/2R$[56], where α is the absorption coefficient, S the scattering coefficient, and R the reflectance. Photoluminescent excitation (PLE), PL spectra and PL decay spectra were recorded on an Edinburgh FLS1000 UV/V/NIR fluorescence spectrometer. PLQY of the title compounds were measured by the FLSP920(EI) fluorescence spectrometer.

2.1 Synthesis of $[Prmim]_3SbCl_6$ (1)

A mixture of $SbCl_3$ (0.2335 g, 1 mmol) and [Prmim]Cl (0.4882 g, 3 mmol) was sealed into a 28 mL Teflon-lined stainless-steel autoclave. In this reaction system, the ionic liquid [Prmim]Cl acts as both solvent and template. The container was closed, heated at 120 ℃ for 3 hours, and then cooled to room temperature naturally. Colourless and transparent block-like crystals were formed after certain time (around two weeks) at room temperature. Long crystallization time possibly relates to the viscosity of the ILs. Once the crystal nuclei were formed, many crystals would be precipitated, and finally **1** could be obtained in a high yield (yield: 0.7042 g, 97% based on Sb). Elemental analysis: calcd. (%) for $C_{21}H_{39}N_6SbCl_6$: C, 35.52; H, 5.53; N, 11.83. Found: C, 35.70; H, 6.11; N, 11.99.

2.2 Synthesis of $[Hmim]_3SbCl_6$ (2)

A similar synthesis procedure as that for **1** was adopted except that a mixture of $SbCl_3$ (1.1641 g, 5 mmol) and [Hmim]Cl (2.1408 g, 10 mmol) was used. Colourless and transparent block-like crystals were formed with the yield of 3.1045 g (72% based on Sb). Elemental analysis: calcd. (%) for $C_{30}H_{57}N_6SbCl_6$: C, 43.08; H, 6.86; N, 10.04. Found: C, 40.94; H, 6.83; N, 9.70.

2.3 Structure refinements

The colorless-transparent block-like crystals **1** and **2**

were selected for SCXRD experiment with dimensions of 0.39mm × 0.39mm × 0.20mm and 0.50mm × 0.25mm × 0.20mm, respectively. For **1,** a total of 31441 reflections were collected in the range of 1.99 °≤ θ ≤30.31 ° with R_{int} = 0.0371, 15049 of which are independent. Crystal **1** crystallizes in monoclinic, space group *Pn* with *a* = 15.2988(12), *b* = 13.6388(10), *c* = 15.6761(13) Å, β = 98.677(7) °, *V* = 3233.5(4) Å^3, *Z* = 4, D_c = 1.459 g·cm^{-3}, *F*(000) = 1440, μ = 1.370 mm^{-1}, *R* = 0.0589 and *wR* = 0.1366 ($I > 2\sigma(I)$). For **2**, 37899 total reflections were collected in 2.24 °≤ θ ≤29.24 ° region with R_{int} = 0.0946, of which 9758 were independent. Crystal **2** is of hexagonal system, space group $P6_3$ with *a* = 27.7471(6), *b* = 27.7471(6), *c* = 8.9811(2) Å, *V* = 5988.2(3) Å^3, *Z* = 6, D_c = 1.391 g·cm^{-3}, *F*(000) = 2592, μ = 1.121 mm^{-1}, *R* = 0.0420 and *wR* = 0.0726 ($I > 2\sigma(I)$). *SHELX* 2018 package was used to solve and refine the structure on F^2 by full-matrix least-square methods[57]. Selected bond lengths and bond angles of **1** and **2** are shown in Table 1, and selected hydrogen bond parameters in Table 2.

Table 1. Selected Bond Lengths (Å) and Bond Angles (°) for 1 and 2

Compound 1			
Bond	Dist.	Bond	Dist.
Sb(1)−Cl(2)	2.552(3)	Sb(2)−Cl(10)	2.529(3)
Sb(1)−Cl(5)	2.568(3)	Sb(2)−Cl(8)	2.605(4)
Sb(1)−Cl(3)	2.576(4)	Sb(2)−Cl(12)	2.617(4)
Sb(1)−Cl(4)	2.752(4)	Sb(2)−Cl(9)	2.685(4)
Sb(1)−Cl(1)	2.754(4)	Sb(2)−Cl(11)	2.738(4)
Sb(1)−Cl(6)	2.789(3)	Sb(2)−Cl(7)	2.838(4)
Angle	(°)	Angle	(°)
Cl(2)−Sb(1)−Cl(5)	89.77(13)	Cl(10)−Sb(2)−Cl(8)	89.91(13)
Cl(2)−Sb(1)−Cl(3)	87.59(14)	Cl(10)−Sb(2)−Cl(12)	90.11(14)
Cl(5)−Sb(1)−Cl(3)	90.89(14)	Cl(8)−Sb(2)−Cl(12)	92.27(13)
Cl(2)−Sb(1)−Cl(4)	89.57(13)	Cl(10)−Sb(2)−Cl(9)	86.76(13)
Cl(5)−Sb(1)−Cl(4)	178.50(16)	Cl(8)−Sb(2)−Cl(9)	89.21(12)
Cl(3)−Sb(1)−Cl(4)	87.74(13)	Cl(12)−Sb(2)−Cl(9)	176.53(13)
Cl(2)−Sb(1)−Cl(1)	88.75(12)	Cl(10)−Sb(2)−Cl(11)	88.94(13)
Cl(5)−Sb(1)−Cl(1)	87.71(14)	Cl(8)−Sb(2)−Cl(11)	178.46(12)
Cl(3)−Sb(1)−Cl(1)	176.08(15)	Cl(12)−Sb(2)−Cl(11)	88.74(14)
Cl(4)−Sb(1)−Cl(1)	93.62(13)	Cl(9)−Sb(2)−Cl(11)	89.72(13)
Cl(2)−Sb(1)−Cl(6)	178.27(14)	Cl(10)−Sb(2)−Cl(7)	177.55(17)
Cl(5)−Sb(1)−Cl(6)	88.74(12)	Cl(8)−Sb(2)−Cl(7)	88.10(13)
Cl(3)−Sb(1)−Cl(6)	91.55(13)	Cl(12)−Sb(2)−Cl(7)	91.40(13)
Cl(4)−Sb(1)−Cl(6)	91.89(12)	Cl(9)−Sb(2)−Cl(7)	91.79(12)
Cl(1)−Sb(1)−Cl(6)	92.08(12)	Cl(11)−Sb(2)−Cl(7)	93.03(13)
Compound 2			
Bond	Dist.	Bond	Dist.
Sb(1)−Cl(5)	2.5480(15)	Sb(1)−Cl(6)	2.6324(14)
Sb(1)−Cl(1)	2.6136(16)	Sb(1)−Cl(4)	2.7367(15)
Sb(1)−Cl(3)	2.6324(15)	Sb(1)−Cl(2)	2.7880(15)
Angle	(°)	Angle	(°)
Cl(5)−Sb(1)−Cl(1)	89.60(5)	Cl(3)−Sb(1)−Cl(4)	91.94(5)
Cl(5)−Sb(1)−Cl(3)	89.66(5)	Cl(6)−Sb(1)−Cl(4)	85.57(5)
Cl(1)−Sb(1)−Cl(3)	90.41(5)	Cl(5)−Sb(1)−Cl(2)	176.56(5)
Cl(5)−Sb(1)−Cl(6)	88.44(5)	Cl(1)−Sb(1)−Cl(2)	90.00(5)
Cl(1)−Sb(1)−Cl(6)	92.06(5)	Cl(3)−Sb(1)−Cl(2)	93.75(5)
Cl(3)−Sb(1)−Cl(6)	176.88(5)	Cl(6)−Sb(1)−Cl(2)	88.16(4)
Cl(5)−Sb(1)−Cl(4)	89.67(5)	Cl(4)−Sb(1)−Cl(2)	90.59(5)
Cl(1)−Sb(1)−Cl(4)	177.54(5)		

Table 2. Selected Hydrogen Bond Lengths (Å) and Bond Angles (°) for 1 and 2

Compound **1**				
D−H ··A	d(D−H)	d(H ··A)	d(D ··A)	∠DHA
C(1)−H(1A) ··Cl(7)#1	0.93	2.94	3.692(18)	138.8
C(2)−H(2A) ··Cl(5)#2	0.93	2.88	3.743(17)	154.1
C(3)−H(3A) ··Cl(6)	0.93	2.76	3.549(15)	142.7
C(4)−H(4A) ··Cl(7)#1	0.96	2.97	3.822(18)	148.1
C(4)−H(4B) ··Cl(3)	0.96	2.87	3.659(18)	139.8
C(8)−H(8A) ··Cl(1)#3	0.93	2.82	3.585(15)	140.7
C(9)−H(9A) ··Cl(7)#4	0.93	2.79	3.673(15)	160.0
C(10)−H(10A) ··Cl(10)#3	0.93	2.94	3.710(14)	141.4
C(11)−H(11A) ··Cl(4)#3	0.96	2.78	3.631(17)	148.5
C(11)−H(11C) ··Cl(11)#3	0.96	2.78	3.606(17)	144.9
C(12)−H(12A) ··Cl(9)#3	0.97	2.82	3.750(15)	160.9
C(12)−H(12B) ··Cl(12)#4	0.97	2.75	3.617(15)	148.6
C(15)−H(15A) ··Cl(11)#5	0.93	2.77	3.609(19)	151.2
C(16)−H(16A) ··Cl(6)#6	0.93	2.88	3.763(18)	159.9
C(17)−H(17A) ··Cl(8)#7	0.93	2.90	3.549(16)	127.7
C(17)−H(17A) ··Cl(9)#7	0.93	2.89	3.618(16)	135.6
C(19)−H(19A) ··Cl(10)#7	0.97	2.94	3.832(17)	153.2
C(19)−H(19B) ··Cl(3)#6	0.97	2.73	3.616(16)	151.6
C(23)−H(23A) ··Cl(1)	0.93	2.62	3.46(2)	150.0
C(24)−H(24A) ··Cl(9)#8	0.93	2.96	3.68(2)	135.0
C(25)−H(25A) ··Cl(9)#8	0.96	2.56	3.50(3)	165.4
C(25)−H(25B) ··Cl(12)#6	0.96	2.64	3.53(3)	155.9
C(26)−H(26A) ··Cl(6)	0.97	2.72	3.63(3)	156.9
C(27)−H(27B) ··Cl(3)#9	0.97	2.95	3.74(3)	140.4
C(29)−H(29A) ··Cl(1)#3	0.93	2.84	3.56(3)	134.3
C(30)−H(30A) ··Cl(12)#7	0.93	2.84	3.73(3)	162.3
C(31)−H(31A) ··Cl(2)	0.93	2.61	3.34(3)	135.8
C(31)−H(31A) ··Cl(3)	0.93	2.87	3.66(2)	143.6
C(33)−H(33B) ··Cl(8)#7	0.97	2.77	3.56(3)	139.2
C(36)−H(36A ··Cl(2)	0.93	2.39	3.275(19)	158.4
C(38)−H(38A) ··Cl(11)#5	0.93	2.66	3.468(19)	145.5
C(39)−H(39A) ··Cl(7)#5	0.96	2.83	3.60(3)	137.7
Compound **2**				
D−H ··A	d(D−H)	d(H ··A)	d(D ··A)	∠DHA
C(1)−H(1A) ··Cl(5)	0.95	2.72	3.582(7)	151.1
C(2)−H(2A) ··Cl(3)#1	0.95	2.64	3.470(6)	146.3
C(3)−H(3A) ··Cl(4)#2	0.95	2.77	3.573(6)	143.3
C(3)−H(3A) ··Cl(6)#2	0.95	2.91	3.617(6)	132.6
C(4)−H(4A) ··Cl(2)#2	0.98	2.68	3.570(6)	151.8
C(4)−H(4C) ··Cl(1)	0.98	2.90	3.761(7)	146.6
C(5)−H(5A) ··Cl(6)#2	0.99	2.66	3.447(7)	136.9
C(5)−H(5B) ··Cl(3)#1	0.99	2.91	3.808(7)	151.0
C(12)−H(12A) ··Cl(2)#2	0.95	2.75	3.468(6)	132.6
C(13)−H(13A) ··Cl(2)#1	0.95	2.64	3.449(6)	143.1
C(14)−H(14A) ··Cl(6)	0.98	2.79	3.368(6)	118.0
C(14)−H(14C) ··Cl(2)#1	0.98	2.73	3.636(6)	154.1
C(15)−H(15A) ··Cl(1)#1	0.99	2.72	3.590(6)	146.3
C(15)−H(15B) ··Cl(6)#2	0.99	2.78	3.568(6)	137.3
C(15)−H(15A) ··Cl(1)#1	0.99	2.72	3.590(6)	146.3
C(15)−H(15B) ··Cl(6)#2	0.99	2.78	3.568(6)	137.3

To be continued

C(21)−H(21A) ··Cl(4)#1	0.95	2.90	3.683(6)	140.8
C(22)−H(22A) ··Cl(5)#3	0.95	2.86	3.649(6)	141.5
C(23)−H(23A) ··Cl(4)	0.95	2.94	3.714(5)	138.9
C(23)−H(23A) ··Cl(5)	0.95	2.80	3.552(6)	136.2
C(24)−H(24A) ··Cl(4)#1	0.98	2.80	3.736(5)	159.2
C(24)−H(24C) ··Cl(6)	0.98	2.79	3.495(6)	129.4
C(25)−H(25A) ··Cl(4)	0.99	2.86	3.668(6)	139.8
C(25)−H(25B) ··Cl(3)#3	0.99	2.84	3.616(6)	135.7

Compound **1**: Symmetry transformations: #1: *x* + 1/2, –*y* + 2, *z* – 1/2; #2: *x* + 1/2, –*y* + 1, *z* + 1/2; #3: *x* + 1/2, –*y* + 1, *z* – 1/2; #4: *x*, *y* – 1, *z*–1; #5: *x* – 1/2, –*y* + 2, *z* – 1/2; #6: *x* – 1/2, –*y* + 1, *z* – 1/2; #7: *x*, *y*, *z* – 1; #8: *x*, *y* – 1, *z*; #9: *x* – 1/2, –*y* + 1, *z* + 1/2

Compound **2**: Symmetry transformations: #1: *x*, *y*, *z* + 1; #2: *y*, –*x* + *y*, *z* + 1/2; #3: –*x* + 1, –*y* + 1, *z* + 1/2

3 RESULTS AND DISCUSSION

SCXRD analysis reveals that **1** crystallizes in the monoclinic space group of *Pn*. As shown in Fig. 1a, the crystallographic asymmetric unit of **1** consists of six $[Prmim]^+$ cations and two isolated $[SbCl_6]^{3-}$ anions. Each Sb^{3+} atom in the crystal is coordinated with six Cl^- atoms, forming a mononuclear $[SbCl_6]^{3-}$ octahedron. The $[SbCl_6]^{3-}$ units are completely separated from each other by $[Prmim]^+$ cations (Fig. 1b). The bond lengths of Sb–Cl fall in the range of 2.529(3)∼2.838(4) Å (Table 1), close to those in previously reported $[Bzmim]_3SbCl_6$ with a range from 2.4983(19) to 2.8679(19) Å[38]. **1** exhibits a three-dimensional supramolecular network considering the hydrogen bonds among $[SbCl_6]^{3-}$ anions and $[Prmim]^+$ cations (Fig. 1c, Table 2). As there are two unique $[SbCl_6]^{3-}$ octahedra in the crystal with Sb(1) ··· Sb(2) distances of 10.1335(11) Å, the hydrogen bonding environments for them are dissimilar (Fig. 1c). Moreover, PLATON calculations indicate different patterns of $\pi\cdots\pi$ accumulation between two imidazole rings (Fig. 1d, Table 3).

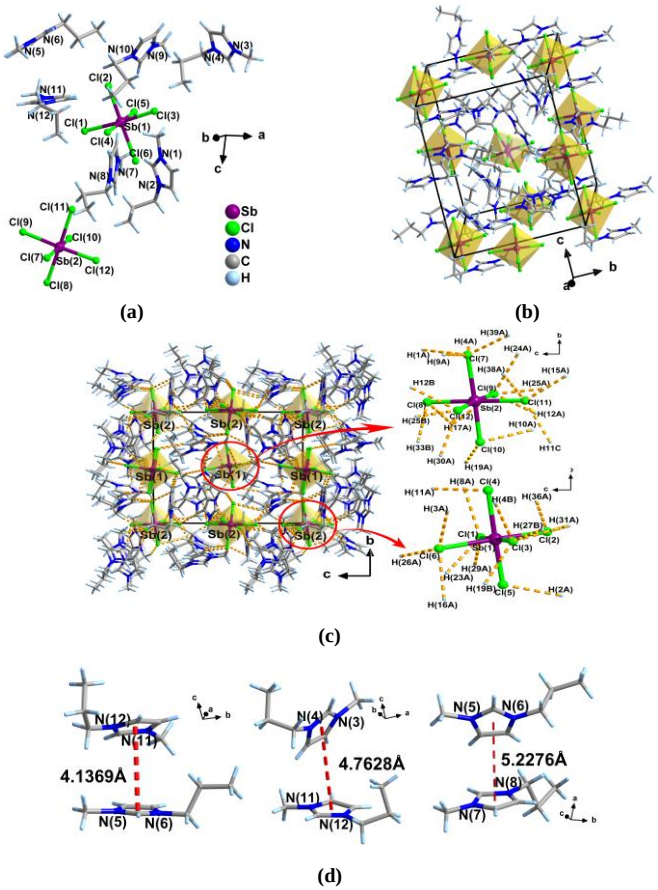

Fig. 1. (a) Asymmetric unit of compound 1. (b) A diagram showing packing of anions and cations in one unit cell of 1. (c) Three-dimensional supramolecular network for 1 considering hydrogen bonds (left) and the hydrogen bonding environment around the $[Sb(1)Cl_6]^{3-}$ and $[Sb(2)Cl_6]^{3-}$ anions (right). (d) Selected $\pi\cdots\pi$ interactions in 1

Table 3. $\pi\cdots\pi$ Interactions in Compound 1

Cg(I)→Cg(J)	Cg ··Cg (Å)	α (°)	β (°)	γ (°)
Cg(3)→Cg(6)	4.1369	26.51	19.68	8.15
Cg(4)→Cg(3)	5.2276	57.60	20.93	78.44
Cg(6)→Cg(2)	4.7628	62.21	9.23	61.86
Cg(6)→Cg(3)	4.1369	26.51	8.15	19.68

Cg(3): N(5)→C(15)→C(16)→N(6)→C(17); Cg(4): N(7)→C(22)→C(23)→N(8)→C(24);
Cg(6): N(11)→C(36)→C(37)→N(12)→C(38)

Single crystal of **2** belongs to the hexagonal space group of $P6_3$ and the crystallographic asymmetric unit contains three $[Hmim]^+$ cations and one $[SbCl_6]^{3-}$ anion, as shown in Fig. 2a. The mononuclear six-coordination $[SbCl_6]^{3-}$ units are surrounded by imidazolium cations with a relatively long hexyl chain, resulting in a 0*D* structure (Fig. 2b). The Sb–Cl bond distances range from 2.5480(15) to 2.7880(15) Å (Table 1), also comparable to those of 2.4983(19)～2.8679(19) Å in $[Bzmim]_3SbCl_6$[38]. Hydrogen bonds are also observed in **2** (Table 2). The detailed hydrogen bonding environment for $[SbCl_6]^{3-}$ anions are presented in Fig. 2c. The isolated $[SbCl_6]^{3-}$ anions are connected to the neighbouring $[Hmim]^+$ cations via C–H ··Cl hydrogen bonds, some of which, such as C(13)–H(13A) ··Cl(2), C(15)–H(13B) ··Cl(6), C(25)–H(25B) ··Cl(3) and C(25)–H(25A) ··Cl(4), result in a 2*D* layer along the *ab* plane (Fig. 2d). Further connected by hydrogen bonds along the *c* axis (*e.g.*, C(24)–H(24A) ··Cl(4) and C(24)–H(24B) ··Cl(6), Fig. 2c), a 3*D* supramolecular structure finally could be obtained. Additionally, $\pi\cdots\pi$ interactions between two imidazole rings in **2** were observed (Fig. 2e, Table 4).

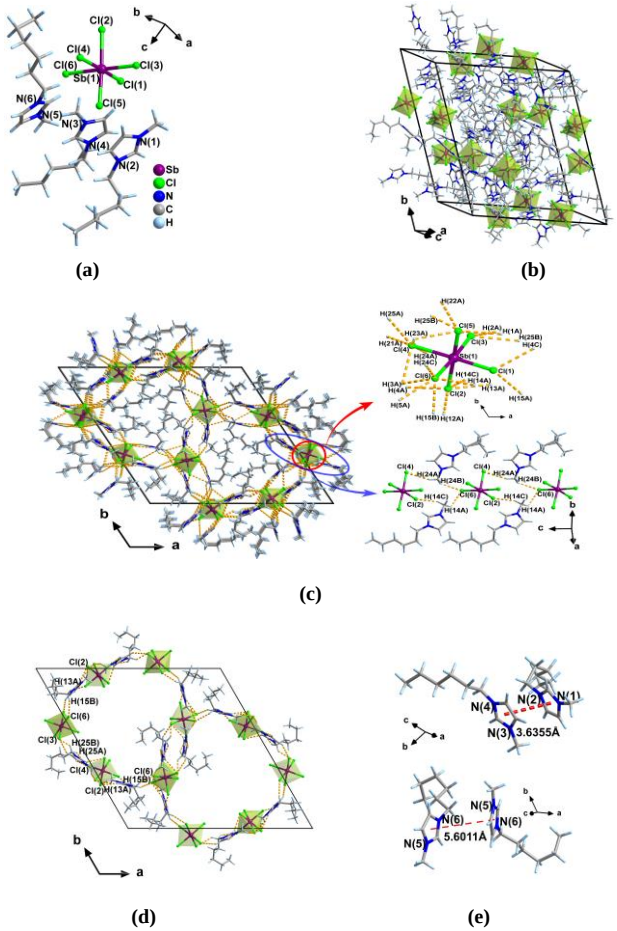

Fig. 2. (a) Asymmetric unit of compound 2. (b) A diagram showing packing of anions and cations in one unit cell of 2. (c) Three-dimensional supramolecular network for 2 considering hydrogen bonds (left) and the hydrogen bonding environment around the $[Sb(1)Cl_6]^{3-}$ anion as well as a one-dimensional supramolecular chain along the *c* axis for 2 considering partial hydrogen bonds (right). (d) Two-dimensional supramolecular network for 2, considering various hydrogen bonds along he *ab* plane. t Partial $[Hmim]^+$ cations and hydrogen bonds are omitted for clarity. (e) Selected $\pi\cdots\pi$ interactions in 2

Table 4. $\pi \cdots \pi$ Interactions in Compound 2

Cg(I)→Cg(J)	Cg ··Cg (Å)	α (°)	β (°)	γ (°)
Cg(1)→Cg(2)	3.6355	6.54	26.46	20.59
Cg(2)→Cg(1)	3.6355	6.54	20.59	26.46
Cg(3)→Cg(3)	5.6011	22.02	43.29	65.06

Cg(1): N(3)→C(11)→C(12)→N(4)→C(13); Cg(2): N(1)→C(1)→C(2)→N(2) →C(3); Cg(3): N(5)→C(21)→C(22)→N(6)→C(23)

The phase purity of the title compounds was confirmed by PXRD (Fig. 3) and EA (Experimental section). TG analyses of **1** and **2** were performed under a N_2 atmosphere from 20 to 800 ℃. As shown in Fig. 4, both compounds display a one-step weight loss from 250 to 370 ℃. Compared with the thermal decomposition procedure of $SbCl_3$ and the corresponding ILs, clearly the thermal properties of the title compounds are highly related to the high thermal stability of ILs.

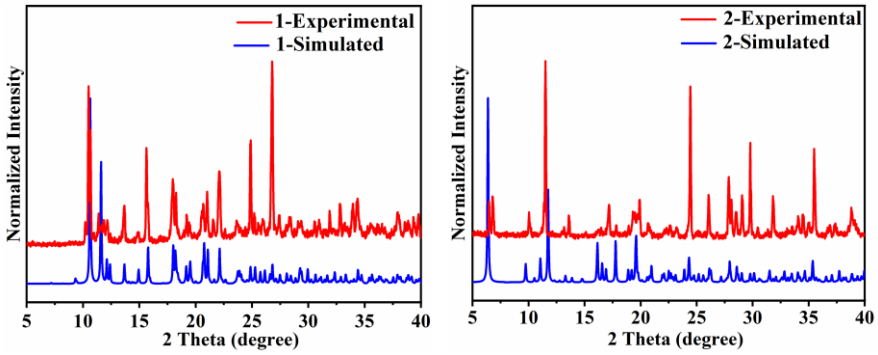

Fig. 3. Comparison of PXRD patterns of the title compounds with the corresponding simulated ones

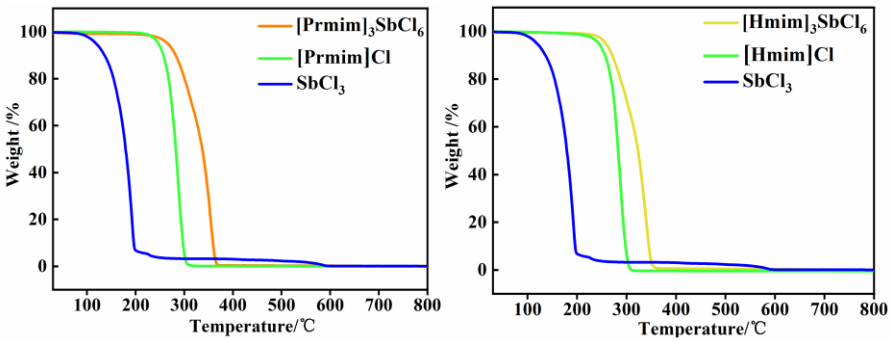

Fig. 4. Comparison of the thermogravimetric curves of the title compounds and $SbCl_3$ as well as the corresponding ionic liquids

The photophysical properties of the title compounds were further characterized by solid-state optical absorption spectra, PLE, PL as well as PL decay spectra at room temperature. As shown in Figs. 5a and 5b, **1** exhibits bright orange emission under the irradiation of 370 nm light, slightly different from **2** which exhibits bright orange-yellow emission under the irradiation of 365 nm light. Both **1** and **2** represent a similarly colorless and transparent appearance under ambient light, suggesting nearly no absorption in the visible region, which is consistent with the optical absorption spectra, as shown in Figs. 5c and 5d. Based on the electron absorption transition of ns^2 electron configuration ions, the two obvious absorption peaks in the absorption spectra can be assigned to $^1S_0 \rightarrow {}^1P_1$ and $^1S_0 \rightarrow {}^3P_1$ transition, respectively[58-60]. The PLE bands of **1** and **2** were consistent with the corresponding optical absorption spectra. Under the excitation of 370 nm light, the PL band of **1** is centered at 627 nm with a large Stokes shift of 257 nm, while the PL band of **2** peaks at 607 nm with a large Stokes shift of 242 nm excited at 365 nm. Broadband emissions of **1** and **2** could be ascribed to $^3P_1 \rightarrow {}^1S_0$ transition from the Sb-based isolated halometallate species[31, 36, 38, 42, 60]. The microsecond PL lifetime for **1** and **2** is in accordance with that of the reported antimony halide hybrids (Figs. 5e and 5f)[38, 42].

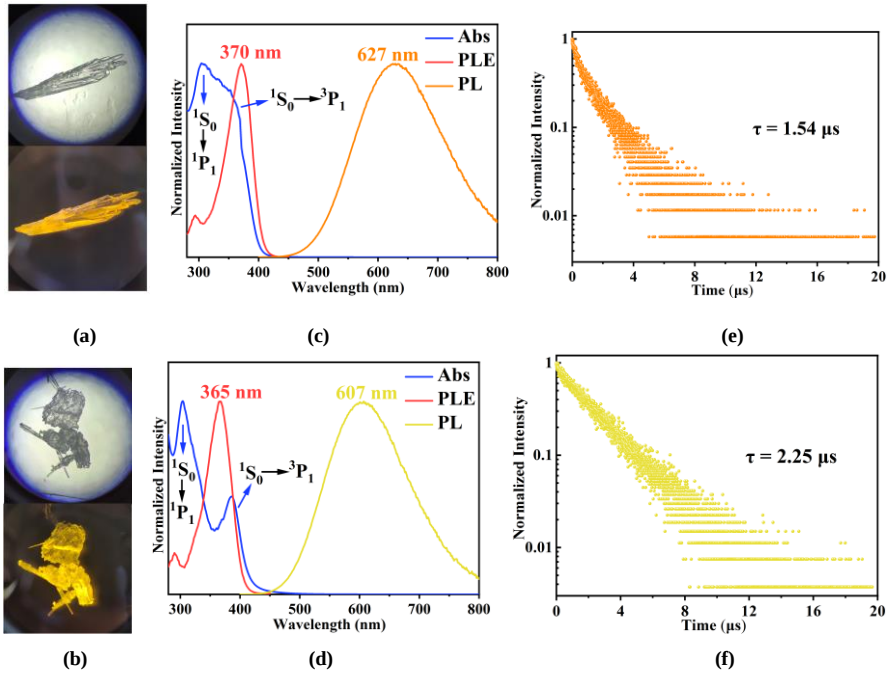

Fig. 5. (a) Single crystal of 1 under ambient light (up) and UV light (down). (b) Single crystal of 2 under ambient light (up) and UV light (down). (c) Optical absorption/PLE/PL spectra for 1. (d) Optical absorption/PLE/PL spectra for 2. (e) PL decay spectra for 1. (f) PL decay spectra for 2

In order to deeply understand the factor that affects the photophysical properties (PL band, Stokes shift, PLQY) of **1** and **2**, the distortion degree of the isolated $[SbCl_6]^{3-}$ unit in the title compounds and corresponding structures in literature was evaluated by using the following formulas[61-63]:

$$\sigma^2 = \frac{1}{11}\sum_{n=1}^{12}(\theta_n - 90°)^2$$

$$\Delta d = \frac{1}{6}\sum_{n=1}^{6}[(d_n - d)/d]^2$$

where θ_n are the Cl−Sb−Cl bond angles, d_n are the Sb−Cl bond lengths, and d is the average of the Sb−Cl bond distances. The results of distortion associated with photophysical properties are summarized in Table 5. It can be found that the PL wavelength and Stokes shift increase with the increasing values of σ^2 and Δd, especially in the case of compounds with a similar organic ligand ($C_6H_{22}N_4$ = tris(2-aminoethyl)amine), which eliminates the influence of organic parts on luminescence. The trend is also observed for the compounds constructed from the ILs with different substituents (*e.g.*, BzmimCl, PrmimCl, and HmimCl). Therefore, the red shift of PL wavelength and larger Stokes shift for **1** should be due to the relatively larger bond length variance (Δd) compared to that for **2**. For PLQY, the trend is in contrast. It is decreasing with more distortion of the halometallate species. The higher extent of structural distortion might lead to more energy dissipation from non-radiative transition in the procedure of excited state reorganization into the symmetric structure, finally resulting in less radiative emission with weak luminescent intensity or weak PLQY in **1**[42]

Table 5. Summary of the Photophysical Characteristics and Distortion Degree of $[SbCl_6]^{3-}$ Octahedron for Selected Hybrid Chloroantimonates (III)

Compounds	PL (nm)	Emission colour	Stokes shift (nm)	PLQY (%)	σ^2	Δd (*10^{-4})	Ref
$[(C_6H_{22}N_4)_2(Sb_2Cl_{10})(SbCl_6)(Cl)_2(H_3O)]\cdot 3(H_2O)$	517	Green	165	45	5.95	0.03	[42]
$(C_6H_{22}N_4)_4(SbCl_6)_3(Cl)_7\cdot 4(H_2O)$	580	Yellow	200	43	9.57	0.18	[42]
$(C_6H_{22}N_4)_2(SbCl_6)_2(Cl)_2\cdot 3(H_2O)$	638	Red	290	6	105.14	90.79	[42]
$(Bzmim)_3SbCl_6$	560	Green	202	87.5	5.54	10.08	[38]
$[Hmim]_3SbCl_6$ (**2**)	607	Orange-yellow	242	49.2	6.91	9.07	Thiswork
$[Prmim]_3SbCl_6$ (**1**)	627	Orange	257	32.5	6.24	14.30	Thiswork

4 CONCLUSION

In summary, by combining $SbCl_3$ and the imidazolium based ILs with different lengths of alkyl chain, two new antimony(III) chloride hybrids featuring a mononuclear $[SbCl_6]^{3-}$ unit were obtained. Compound **1** exhibits bright orange emission peaking at 627 nm with relatively larger Stokes shift of 257 nm. **2** exhibits bright orange-yellow emission peaking at 607 nm with Stokes shift of 242 nm. The PL peak, Stokes shift and PLQY for **1** and **2** are highly related to the extent of distortion of halometallate unit. Our studies enrich the family of $[SbCl_6]^{3-}$ based luminescent IOMHs.

REFERENCES

(1) Gautier, R.; Massuyeau, F.; Galnon, G.; Paris, M. Lead halide post-perovskite-type chains for high-efficiency white-light emission. *Adv. Mater*. **2019**, 31, 1807383–6.

(2) Gong, L. K.; Hu, Q. Q.; Huang, F. Q.; Zhang, Z. Z.; Shen, N. N.; Hu, B.; Song, Y.; Wang, Z. P.; Du, K. Z.; Huang, X. Y. Efficient modulation of photoluminescence by hydrogen bonding interactions between inorganic $[MnBr_4]^{2-}$ anions and organic cations. *Chem. Commun.* **2019**, 55, 7303–7306.

(3) Lin, H. R.; Zhou, C. K.; Tian, Y.; Siegrist, T.; Ma, B. W. Low-dimensional organometal halide perovskites. *ACS Energy Lett.* **2017**, 3, 54–62.

(4) Saidaminov, M. I.; Mohammed, O. F.; Bakr, O. M. Low-dimensional-networked metal halide perovskites: the next big thing. *ACS Energy Lett.* **2017**, 2, 889–896.

(5) Shen, N. N.; Wang, Z. P.; Jin, J. C.; Gong, L. K.; Zhang, Z. Z.; Huang, X. Y. Phase transitions and photoluminescence switching in hybrid antimony(III) and bismuth(III) halides. *CrystEngComm*. **2020**, 22, 3395–3405.

(6) Tsai, H. H.; Nie, W. Y.; Blancon, J. C.; Toumpos, C. S.; Asadpour, R.; Harutyunyan, B.; Neukirch, A. J.; Verduzco, R.; Crochet, J. J.; Tretiak, S.; Pedesseau, L.; Even, J.; Alam, M. A.; Gupta, G.; Lou, J.; Ajayan, P. M.; Bedzyk, M. J.; Kanatzidis, M. G.; Mohite, A. D. High-efficiency two-dimensional Ruddlesden-Popper perovskite solar cells. *Nature* **2016**, 536, 312–316.

(7) Worku, M.; Tian, Y.; Zhou, C. K.; Lee, S.; Meisner, Q.; Zhou, Y.; Ma, B. W. Sunlike white-light-emitting diodes based on zero-dimensional organic metal halide hybrids. *ACS Appl. Mater. Interfaces* **2018**, 10, 30051–30057.

(8) Xuan, T. T.; Xie, R. J. Recent processes on light-emitting lead-free metal halide perovskites. *Chem. Eng. J.* **2020**, 393, 124757–20.

(9) Zhou, C. K.; Lin, H. R.; He, Q. Q.; Xu, L. J.; Worku, M.; Chaaban, M.; Lee, S. J.; Shi, X. Q.; Du, M. H.; Ma, B. W. Low dimensional metal halide perovskites and hybrids. *Mater. Sci. Eng. R* **2019**, 137, 38–65.

(10) Zhou, C. K.; Lin, H. R.; Lee, S. J.; Chaaban, M.; Ma, B. W. Organic-inorganic metal halide hybrids beyond perovskites. *Mater. Res. Lett.* **2018**, 6, 552–569.

(11) Li, M. Z.; Xia, Z. G. Recent progress of zero-dimensional luminescent metal halides. *Chem. Soc. Rev.* **2021** DOI: 10.1039/d0cs00779j.

(12) Wang, X. M.; Meng, W. W.; Liao, W. Q.; Wang, J. B.; Xiong, R. G.; Yan, Y. F. Atomistic mechanism of broadband emission in metal halide perovskites. *J. Phys. Chem. Lett.* **2019**, 10, 501–506.

(13) Zhou, C. K.; Xu, L. J.; Lee, S. J.; Lin, H. R.; Ma, B. W. Recent advances in luminescent zero-dimensional organic metal halide hybrids. *Adv. Opt. Mater.* **2020**, 2001766–17.

(14) Zhou, G. J.; Su, B. B.; Huang, J. L.; Zhang, Q. Y.; Xia, Z. G. Broad-band emission in metal halide perovskites: mechanism, materials, and applications. *Mater. Sci. Eng. R* **2020**, 141, 100548–21.

(15) Benin, B. M.; Dirin, D. N.; Morad, V.; Worle, M.; Yakunin, S.; Raino, G.; Nazarenko, O.; Fischer, M.; Infante, I.; Kovalenko, M. V. Highly emissive self-trapped excitons in fully inorganic zero-dimensional tin halides. *Angew. Chem. Int. Ed.* **2018**, 57, 11329–11333.

(16) Dohner, E. R.; Jaffe, A.; Bradshaw, L. R.; Karunadasa, H. I. Intrinsic white-light emission from layered hybrid perovskites. *J. Am. Chem. Soc.* **2014**, 136, 13154–13157.

(17) Fu, P. F.; Huang, M. L.; Shang, Y. Q.; Yu, N.; Zhou, H. L.; Zhang, Y. B.; Chen, S. Y.; Gong, J. K.; Ning, Z. J. Organic-inorganic layered and hollow tin bromide perovskite with tunable broadband Emission. *ACS Appl. Mater. Interfaces* **2018**, 10, 34363–34369.

(18) Kshirsagar, A. S.; Nag, A. Synthesis and optical properties of colloidal $Cs_2AgSb_{1-x}Bi_xCl_6$ double perovskite nanocrystals. *J. Chem. Phys.* **2019**, 151, 161101–6.

(19) Mao, L. L.; Guo, P. J.; Kepenekian, M.; Hadar, I.; Katan, C.; Even, J.; Schaller, R. D.; Stoumpos, C. C.; Kanatzidis, M. G. Structural diversity in white-light-emitting hybrid lead bromide perovskites. *J. Am. Chem. Soc.* **2018**, 140, 13078–13088.

(20) Morad, V.; Shynkarenko, Y.; Yakunin, S.; Brumberg, A.; Schaller, R. D.; Kovalenko, M. V. Disphenoidal zero-dimensional lead, tin, and germanium halides: highly emissive singlet and triplet self-trapped excitons and X-ray scintillation. *J. Am. Chem. Soc.* **2019**, 141, 9764–9768.

(21) Song, G. M.; Li, M. Z.; Yang, Y.; Liang, F.; Huang, Q.; Liu, X. M.; Gong, P. F.; Xia, Z. G.; Lin, Z. S. Lead-free tin(IV)-based organic-inorganic metal halide hybrids with excellent stability and blue-broadband emission. *J. Phys. Chem. Lett.* **2020**, 11, 1808−1813.

(22) Su, B. B.; Song, G. M.; Molokeev, M. S.; Lin, Z. S.; Xia, Z. G. Synthesis, crystal structure and green luminescence in zero-dimensional tin halide $(C_8H_{14}N_2)_2SnBr_6$. *Inorg. Chem.* **2020**, 58, 9962−9968.

(23) Tan, Z. F.; Li, J. H.; Zhang, C.; Li, Z.; Hu, Q. S.; Xiao, Z. W.; Kamiya, T.; Hosono, H.; Niu, G.; Lifshitz, E.; Cheng, Y.; Tang, J. Highly efficient blue-emitting bi-doped Cs_2SnCl_6 perovskite variant: photoluminescence induced by impurity doping. *Adv. Funct. Mater.* **2018** 1801131−10.

(24) Yangui, A.; Roccanova, R.; Wu, Y.; Du, M. H.; Saparov, B. Highly efficient broad-band luminescence involving organic and inorganic molecules in a zero-dimensional hybrid lead chloride. *J. Phys. Chem. C* **2019**, 123, 22470−22477.

(25) Zhao, Y.; Zhou, C. K.; Tian, Y.; Shu, Y.; Messier, J.; Wang, J. C.; Van De Burgt, L. J.; Kountouriotis, K.; Xin, Y.; Holt, E.; Schanze, K.; Clark, R.; Siegrist, T.; Ma, B. W. One-dimensional organic lead halide perovskites with efficient bluish white-light emission. *Nat. Commun.* **2017**, 8, 14051−7.

(26) Zhang, R. L.; Mao, X.; Yang, Y.; Yang, S. Q.; Zhao, W. Y.; Wumaier, T.; Wei, D. H.; Deng, W. Q.; Han, K. L. Air-stable, lead-free zero-dimensional mixed bismuth-antimony perovskite single crystals with ultra-broadband emission. *Angew. Chem. Int. Ed.* **2019**, 58, 2725−2729.

(27) Zhou, C. K.; Lin, H. R.; Neu, J.; Zhou, Y.; Chaaban, M.; Lee, S. J.; Worku, M.; Chen, B. H.; Clark, R.; Cheng, W. H.; Guan, J. J.; Djurovich, P.; Zhang, D. Z.; Lü, X. J.; Bullock, J.; Pak, C.; Shatruk, M.; Du, M. H.; Siegrist, T.; Ma, B. W. Green emitting single-crystalline bulk assembly of metal halide clusters with near-unity photoluminescence quantum efficiency. *ACS Energy Lett.* **2019**, 4, 1579−1583.

(28) Zhou, C. K.; Lin, H. R.; Shi, H. L.; Tian, Y.; Pak, C.; Shatruk, M.; Zhou, Y.; Djurovich, P.; Du, M. H.; Ma, B. W. A zero-dimensional organic seesaw-shaped tin bromide with highly efficient strongly stokes-shifted deep-red emission. *Angew. Chem. Int. Ed.* **2017**, 57, 1021−1024.

(29) Zhou, C. K.; Lin, H. R.; Worku, M.; Neu, J.; Zhou, Y.; Tian, Y.; Lee, S. J.; Djurovich, P.; Siegrist, T.; Ma, B. W. Blue emitting single crystalline assembly of metal halide clusters. *J. Am. Chem. Soc.* **2018**, 140, 13181−13184.

(30) Zhou, C. K.; Tian, Y.; Wang, M. C.; Rose, A.; Besara, T.; Doyle, N. K.; Yuan, Z.; Wang, J. C.; Clark, R.; Hu, Y. Y.; Siegrist, T.; Lin, S. C.; Ma, B. W. Low-dimensional organic tin bromide perovskites and their photoinduced structural transformation. *Angew. Chem. Int. Ed.* **2017**, 56, 9018−9022.

(31) Li, Z. Y.; Li, Y.; Liang, P.; Zhou, T. L.; Wang, L.; Xie, R. J. Dual-band luminescent lead-free antimony chloride halides with near-unity photoluminescence quantum efficiency. *Chem. Mater.* **2019**, 31, 9363−9371.

(32) Elleuch, N.; Lhoste, J.; Boujelbene, M. Characterization, Hirshfeld surface analysis and vibrational properties of 2,6-diaminopurinium chloride tetrachloroantimonates(III) monohydrate $(C_5H_8N_6)[SbCl_4]Cl{\cdot}H_2O$. *J. Mol. Struct.* **2020**, 1217, 128386−11.

(33) He, Q. Q.; Zhou, C. K.; Xu, L. J.; Lee, S. J.; Lin, X. S.; Neu, J.; Worku, M.; Chaaban, M.; Ma, B. W. Highly stable organic antimony halide crystals for X-ray scintillation. *ACS Mater. Lett.* **2020**, 2, 633−638.

(34) Morad, V.; Yakunin, S.; Kovalenko, M. V. Supramolecular approach for fine-tuning of the bright luminescence from zero-dimensional antimony(III) halides. *ACS Mater. Lett.* **2020**, 2, 845−852.

(35) Sedakova, T. V.; Mirochnik, A. G. Luminescence of antimony(III) halogenides complexes with 2-and 4-benzylpyridine. *Russ. J. Phys. Chem. A* **2017**, 91, 791−795.

(36) Song, G. M.; Li, M. Z.; Zhang, S. Z.; Wang, N. Z.; Gong, P. F.; Xia, Z. G.; Lin, Z. S. Enhancing photoluminescence quantum yield in 0*D* metal halides by introducing water molecules. *Adv. Funct. Mater.* **2020**, 30, 2002468−6.

(37) Wang, Z. P.; Xie, D. L.; Zhang, F.; Yu, J. B.; Chen, X. P.; Wong, C. P. Controlling information duration on rewritable luminescent paper based on hybrid antimony(III) chloride/small-molecule absorbates. *Sci. Adv.* **2020**, 6, eabc2181−10.

(38) Wang, Z. P.; Zhang, Z. Z.; Tao, L. Q.; Shen, N. N.; Hu, B.; Gong, L. K.; Li, J. R.; Chen, X. P.; Huang, X. Y. Hybrid chloroantimonates(III): thermally induced triple-mode reversible luminescent switching and laser-printable rewritable luminescent paper. *Angew. Chem. Int. Ed.* **2019**, 58, 9974–9978.

(39) Wang, Z. P.; Wang, J. Y.; Li, J. R.; Feng, M. L.; Zou, G. D.; Huang, X. Y. $[Bmim]_2SbCl_5$: a main group metal-containing ionic liquid exhibiting tunable photoluminescence and white-light emission. *Chem. Commun.* **2015**, 51, 3094–3097.

(40) Zhou, C. K.; Lin, H. R.; Tian, Y.; Yuan, Z.; Clark, R.; Chen, B. H.; Van De Burgt, L. J.; Wang, J. C.; Zhou, Y.; Hanson, K.; Meisner, Q. J.; Neu, J.; Besara, T.; Siegrist, T.; Lambers, E.; Djurovich, P.; Ma, B. W. Luminescent zero-dimensional organic metal halide hybrids with near-unity quantum efficiency. *Chem. Sci.* **2018**, 9, 586–593.

(41) Zhou, C. K.; Worku, M.; Neu, J.; Lin, H. R.; Tian, Y.; Lee, S. J.; Zhou, Y.; Han, D.; Chen, S. Y.; Hao, A.; Djurovich, P. I.; Siegrist, T.; Du, M. H.; Ma, B. W. Facile preparation of light emitting organic metal halide crystals with near-unity quantum efficiency. *Chem. Mater.* **2018**, 30, 2374–2378.

(42) Biswas, A.; Bakthavatsalam, R.; Mali, B. P.; Bahadur, V.; Biswas, C.; Raavi, S. S. K.; Gonnade, R. G.; Kundu, J. The metal halide structure and the extent of distortion control the photo-physical properties of luminescent zero dimensional organic-antimony(III) halide hybrids. *J. Mater. Chem. C*

2021, 9, 348−358.

(43) Chen, F.; Wang, S.; Li, Y. H.; Huang, W. Effects of anionic geometries on hydrogen-bonding networks of 1-(4-pyridyl) piperazine. *J. Chem. Crystallogr.* **2016**, 46, 309−323.

(44) Wojciechowska, M.; Szklarz, P.; Bialonska, A.; Baran, J.; Janicki, R.; Medycki, W.; Durlak, P.; Piecha-Bisiorek, A.; Jakubas, R. Enormous lattice distortion through an isomorphous phase transition in an organic-inorganic hybrid based on haloantimonate(III). *CrystEngComm*. **2016**, 18, 6184−6194.

(45) Parmar, S.; Pal, S.; Biswas, A.; Gosavi, S.; Chakraborty, S.; Reddy, M. C.; Ogale, S. Designing a new family of oxonium-cation based structurally diverse organic-inorganic hybrid iodoantimonate crystals. *Chem. Commun.* **2019**, 55, 7562−7565.

(46) Wojtas, M.; Jakubas, R.; Ciunik, Z.; Medycki, W. Structure and phase transitions in $[(CH_3)_4P]_3Sb_2Br_9$ and $[(CH_3)_4P]_3Bi_2Br_9$. *J. Solid State Chem.* **2004**, 177, 1575−1584.

(47) Benin, B. M.; Mccall, K. M.; Worle, M.; Morad, V.; Aebli, M.; Yakunin, S.; Shynkarenko, Y.; Kovalenko, M. V. The $Rb_7Bi_{3-3x}Sb_{3x}Cl_{16}$ family: a fully inorganic solid solution with room-temperature luminescent members. *Angew. Chem. Int. Ed.* **2020**, 59, 14490−14497.

(48) Plecha, A.; Pietraszko, A.; Bator, G.; Jakubas, R. Structural characterization and ferroelectric ordering in $(C_3N_2H_5)_5Sb_2Br_{11}$. *J. Solid State Chem.* **2008**, 181, 1155−1166.

(49) Ma, Z.; Yu, J. H.; Dai, S. Preparation of inorganic materials using ionic liquids. *Adv. Mater.* **2010**, 22, 261−285.

(50) Olivier-Bourbigou, H.; Magna, L.; Morvan, D. Ionic liquids and catalysis: recent progress from knowledge to applications. *Appl. Catal. A-Gen.* **2010**, 373, 1−56.

(51) Plechkova, N. V.; Seddon, K. R. Applications of ionic liquids in the chemical industry. *Chem. Soc. Rev.* **2008**, 37, 123−150.

(52) Zhang, S. G.; Zhang, Q. H.; Zhang, Y.; Chen, Z. J.; Watanabe, M.; Deng, Y. Q. Beyond solvents and electrolytes: Ionic liquids-based advanced functional materials. *Prog. Mater. Sci.* **2016**, 77, 80−124.

(53) Li, H. R.; Liu, P.; Shao, H. F.; Wang, Y. G.; Zheng, Y. X.; Sun, Z.; Chen, Y. H. Green synthesis of luminescent soft materials derived from task-specific ionic liquid for solubilizing lanthanide oxides and organic ligand. *J. Mater. Chem.* **2009**, 19, 5533−5540.

(54) Torimoto, T.; Tsuda, T.; Okazaki, K.; Kuwabata, S. New frontiers in materials science opened by ionic liquids. *Adv. Mater.* **2010**, 22, 1196−1221.

(55) Ichikawa, T.; Kato, T.; Ohno, H. Dimension control of ionic liquids. *Chem. Commun.* **2019**, 55, 8205−8214.

(56) Wendlandt, W. M.; Hecht, H. G. *Reflectance Spectroscopy*. Interscience, New York **1966**.

(57) Sheldrick, G. M. Crystal structure refinement with *SHELXL*. *Acta Crystallogr. Sect. C* **2015**, 71, 3–8.

(58) Vogler, A.; Nikol, H. Photochemistry and photophysics of coordination compounds of the main group metals. *Pure Appl. Chem.* **1992**, 64, 1311−1317.

(59) Nikol, H.; Vogler, A. Photoluminescence of antimony(III) and bismuth(III) complexes in solution. *J. Am. Chem. Soc.* **1991**, 113, 8988−8990.

(60) Vogler, A.; Nikol, H. The structures of s^2 metal complexes in the ground and sp excited states. *Comments Inorg. Chem.* **1993**, 14, 245−261.

(61) Robinson, K.; Gibbs, G. V.; Ribbe, P. H. Quadriatic elongation-quantitative measure of distortion in coordination polyhedra. *Science* **1971**, 172, 567−570.

(62) Yin, J. L.; Zhang, G. Y.; Peng, C. D.; Fei, H. H. An ultrastable metal-organic material emits efficient and broadband bluish white-light emission for luminescent thermometers. *Chem. Commun.* **2019**, 55, 1702−1705.

(63) Zhou, L.; Liao, J. F.; Huang, Z. G.; Wei, J. H.; Wang, X. D.; Chen, H. Y.; Kuang, D. B. Intrinsic self-trapped emission in 0*D* lead-free $(C_4H_{14}N_2)_2In_2Br_{10}$ single crystal. *Angew. Chem. Int. Ed.* **2019**, 58, 15435−15440.